ELSEVIER

Contents lists available at ScienceDirect

Carbohydrate Polymer Technologies and Applications



journal homepage: www.sciencedirect.com/journal/carbohydrate-polymer-technologies-and-applications

Double cross-linking oxidized sodium alginate with Ag-based metal-organic framework and borax as an antibacterial spray-filming hydrogel for bacterial barrier

Siamak Javanbakht . Reza Mohammadi * 💿

Polymer Research Laboratory, Department of Organic and Biochemistry, Faculty of Chemistry, University of Tabriz, Transcript, T

ARTICLE INFO

Keywords: Alginate Dual network Metal-organic framework Antibacterial Spray-filming hydrogels

ABSTRACT

Hydrogels with spray-filming ability still face difficulties preventing infections, mainly when used on mass wounds. These challenges arise due to their lack of flexibility, antibacterial activity, and slow protective film formation on the wound. This study developed a spray-filming hydrogel using an amine-functionalized silverbased metal-organic framework (Ag-MOF), oxidized alginate (O-Alg), and borax (BX). The designed double cross-linked O-Alg/Ag-MOF/BX hydrogel exhibited superior spray-filming ability by utilizing dynamic Schiff base and boronic ester bonds. Various methods were employed to analyze and confirm the structure and characteristics of the hydrogel films. Furthermore, the gelation process of O-Alg/Ag-MOF/BX hydrogel was found to occur within 5–30 s, allowing for rapid film formation through spray application of the two-precursor mixture. An antibacterial study showed significant activity against gram-negative and positive bacteria, with an inhibition zone measuring about 1.3 ± 0.1 cm. Notably, the bacterial barriers test demonstrated that the O-Alg/Ag-MOF/BX hydrogel films effectively prevented the growth of *E. coli* and *S. aureus* for 12 h The hydrogels also exhibited good cytocompatibility with human skin fibroblast cells (HFF-1, over 70 % cell viability). As a result, the O-Alg/Ag-MOF/BX hydrogel holds a promising bio-platform for potential use in wound dressings, particularly in scenarios involving large and irregularly shaped injuries.

1. Introduction

Hydrogels are wet and soft materials with a 3D network structure and distinctive physical properties such as an adjustable porous structure, softness, and water retention (Yang, 2022). They possess good biocompatibility and have been extensively used in various fields, including tissue engineering (Zhao et al., 2020), wound dressings (Tawre et al., 2024), drug delivery (Kesharwani et al., 2021), diagnostics (Cha et al., 2022), regenerative medicine (Tayler & Stowers, 2021), and medical devices (Hachimi Alaoui & Fatimi, 2023). Hydrogels are extensively utilized due to their structural resemblance to biological extracellular matrix (ECM) and their capacity to conform to irregular wound contours (Zheng et al., 2020; Wu et al., 2023). Furthermore, these materials foster an optimal milieu for epidermal regeneration while establishing a barrier against moisture evaporation and wound contamination (da Silva et al., 2019). Nevertheless, conventional hydrogels exhibit deficiencies in tissue adhesion, mechanical integrity, and abrasion resistance, resulting in various limitations, including incompatibility with wound morphology, insufficient functionality, inadequate degradation rates, and unpredictable therapeutic outcomes (Li et al., 2024). Additionally, traditional hydrogels often forfeit injection and spray-filming ability, complicating their abrasive resistance, shape conformity, and functional enhancement (Shu et al., 2024). Hydrogel wound dressings have a unique spray-filming ability that could offer durable effects for the treatment of wounds (Jeong et al., 2024).

In general, the forming hydrogel is reliant upon both noncovalent (physical) and covalent (chemical) reactions among the polymeric chains to form the hydrogel (Zheng et al., 2021; Teng et al., 2019). Among the various covalent reactions, Schiff base cross-linking stands out due to its capacity for dynamic reversibility, rapid *in-situ* cross-linking, and environmental responsiveness to changes in pH (Mo et al., 2021; Pawariya et al., 2023). Consequently, Schiff base cross-linking has frequently been utilized to generate hydrogels for wound dressings purposes, including agarose/PEG (Zhang et al., 2018), PEG/chitosan (Ren et al., 2018), and PAM/alginate (Chen et al., 2018),

E-mail address: r.mohammadi@tabrizu.ac.ir (R. Mohammadi).

https://doi.org/10.1016/j.carpta.2024.100629

^{*} Corresponding author.

owing to their several benefits such as fast formation, pH responsiveness, compatibility with living cells, tissue adhesiveness. While such hydrogels primarily cater to healing wounds by either injection or direct applications such as gauze, limited research focuses on their use during mass casualty conditions in prehospital trauma, such as road accidents, war, and natural calamities, where they could effectively protect mass or irregular traumas amid infectious outbreaks. A hydrogel with a spray-filming capability must be developed to address this issue, enabling their straight application in prehospital trauma. Besides, such hydrogel films would prevent bacterial infections and secondary injuries during the prehospital phase, increasing the chances of survival and reducing complications. Consequently, spray-filming hydrogels hold great potential in serving as an excellent wound dressing for covering and shielding wounds.

To the extent of our understanding, few hydrogels possess the qualities of spray-filming ability. Previous studies have also noted the

characteristics of a particular hydrogel, named SA-CHO/Gel, composed of gelatin (Gel)/oxidized sodium alginate (SA-CHO) with a gelation time of 7500 s. The presence of borax (BX) can quicken its gelation time to ≈20 s (Balakrishnan et al., 2014), but this hydrogel cannot be sprayed due to its extended gelation period. Another study described a hydrogel based on monoaldehyde-modified sodium alginate (SA-mCHO) and adipic acid dihydrazidemodified gelatin (Gel-ADH) to resolve this issue. The hydrogels showed a rapid gelation time of 2–21 s using Schiff base bonds. The prepared hydrogel films could form an effective barrier to Candida albicans and Staphylococcus aureus for 12 h; however, they had no bactericidal effect (Du et al., 2020). Nanoparticles can enhance hydrogel properties, including their bioactivity and physicochemical properties (Li et al., 2019; Hong et al., 2022; Zengin et al., 2021). For example, incorporating nanoscale metal-organic frameworks (MOFs) into hydrogels improves their biomedical and mechanical properties (Li et al., 2021; Zeng et al., 2022). MOFs are porous materials that can be

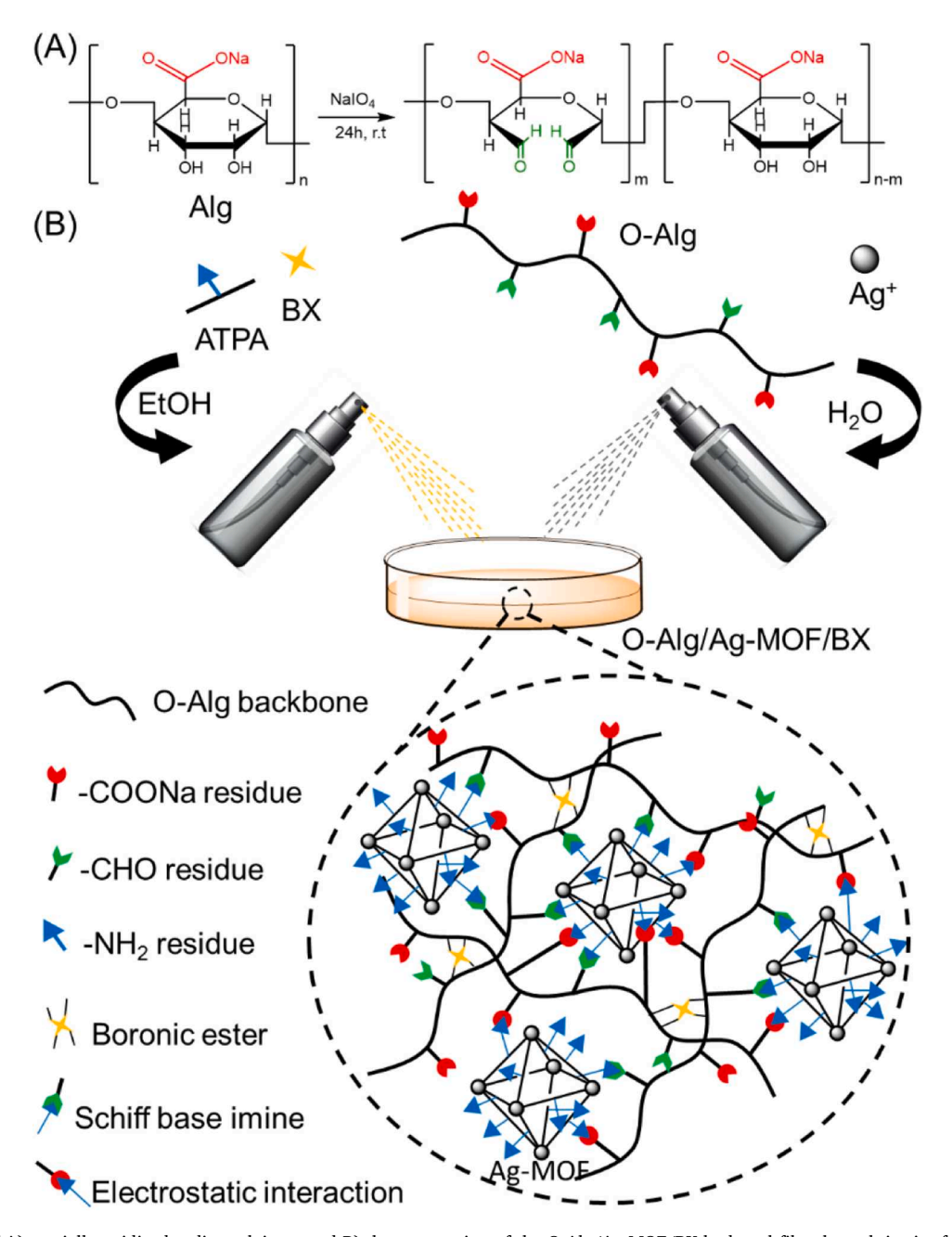


Fig. 1. Schematic of A) partially oxidized sodium alginate and B) the preparation of the O-Alg/Ag-MOF/BX hydrogel film through in-situ forming Ag-MOF, electrostatic interaction, boronic ester, and Schiff base reactions.

used for various applications (Sohrabi et al., 2021; Mansour et al., 2024). MOFs' porous structure and high surface area allow strong interactions with the hydrogel matrix, improving strength and toughness. Incorporating antibacterial MOFs into the hydrogel matrix could improve its antibacterial properties, as the MOFs can release antibacterial agents over time (Li et al., 2021). This could lead to better wound healing outcomes and prevent bacterial infections.

Hence, this work aimed to prepare an antibacterial spray-filming hydrogel film, a double cross-linked hydrogel designed based on Schiff base imine and boronic esterification reaction. The target hydrogel (O-Alg/Ag-MOF/BX) was obtained by in-situ forming antibacterial aminfunctionalized Ag-based metal-organic framework (Ag-MOF) and accordingly reacting within oxidized alginate (O-Alg) through Schiff base reaction and followed by esterification with borax (BX), Fig. 1. On the other hand, the synthesis of the O-Alg/Ag-MOF/BX hydrogel was achieved through a cross-linking reaction that incorporated O-Alg, BX, and amine-functionalized Ag-MOF. This innovative approach not only facilitated the formation of a robust hydrogel network but also significantly enhanced its spray-filming ability. Then, the physical and chemical structures of the hydrogels were characterized by different analysis techniques. Besides, the spray-filming properties, gelation time, antibacterial activity, and cytotoxicity of the O-Alg/Ag-MOF/BX hydrogel were studied, and their potential was evaluated as bacterial barriers and antibacterial wound dressing. The dynamic Schiff base and boronic ester bonds formed during the cross-linking process contribute to the hydrogel's flexibility and durability, which are crucial for effective wound coverage, particularly in irregular and mass wounds. These properties are essential for maintaining a protective barrier against infections while allowing for ease of application in emergency settings.

2. Experimental methods

2.1. Materials

Sodium alginate (SA, Mw \approx 236 kDa, 98 %), sodium hydroxide (NaOH, 99 %), sodium periodate (NaIO₄, 99.5 %), silver acetate (AgOAc. 99 %), terephthalic acid (TPA, 98 %), 2,4-dinitrophenylhydrazine (DNPH, 97 %), and all other chemicals were obtained from Merck Co. All biological agents were attained from Sigma Aldrich Co., USA.

2.2. Preparation of O-Alg/Ag-MOF/BX hydrogel

A mixture containing 2 % w/v of O-Alg (oxidation of Alg was described in SI) and 0.2 mM AgOAc in 10 mL of distilled water was prepared. Another mixture containing 0.2 mM aminoterephthalic acid (ATPA, detailed synthesis described in supporting information) and 0.1 mM borax in 10 mL of EtOH/H $_2$ O (1:1) was prepared (Y). Then, these two mixtures were alternately sprayed on the desired surface (except for the glass side using conventional sprayers) until they completely covered the surface with approximately 30 sprays of each mixture. After gelation for about 30 s, it was dried at ambient temperature for 12 h The control sample Alg/BX was prepared according to the above method, with the difference that Alg was used instead of O-Alg, and AgOAc and ATPA were not added to the sprayed mixtures.

2.3. Characterization of hydrogel

Various analyses were employed to characterize the samples. An FT-IR spectrometer (Bruker Instruments, model Aquinox 55, Germany) was used to obtain infrared spectra of the samples. UV–vis absorption spectra of the samples were obtained using a spectrophotometer (Shimadzu, model 2450). The fluorescent properties of the films were examined through the utilization of a spectrofluorometer (FP-6200, JASCO). Additionally, the surface morphology of the samples was investigated with the aid of a scanning electron microscope (SEM; LEO, 1430VP) and atomic force microscopy (AFM, FLEX, Nanosurf, Swiss). Moreover, the

samples' tensile strength and elongation at break were determined using a universal testing machine (Zwick/Roell, Model, Z010 Germany).

The duration of gelation for O-Alg/Ag-MOF/BX hydrogels with varying spraying volume ratios was ascertained using the simple vial-tilting technique. This was done to determine if the system fulfilled the criteria for speedy film formation, as established in the literature (Wang et al., 2011). The mean value was presented along with the standard deviation based on a sample size of three. Statistical significance was deemed to be attained if the p-value was lower than 0.05.

The process of analyzing swelling and erosion involved immersing measured samples of identical sizes in 10 mL of PBS with pH 7.4 at 37 $^{\circ}$ C (physiological temperature), mimicking wound exudate. The swollen films were then removed from the solution and weighed after removing any surface water at specified intervals by blotting them onto filter paper. To estimate erosion, the films were left to dry at room temperature for 24 h and then reweighed. The swelling (calculated using Eq. (1)) and erosion (calculated using Eq. (2)) ratio was determined as:

$$Swelling \ ratio = \frac{Wt - Wi}{Wi} \tag{1}$$

where W_i = initial dry weight and W_t = weight of wet hydrogels at time t.

$$Erosion = \frac{Wi - Wt(d)}{Wi} \times 100\%$$
 (2)

where $W_t(d)$ = dry weight of hydrogels at time t.

The gravimetrical technique was utilized to evaluate the prepared films' water vapor permeability (WVP, $g\cdot m \cdot 1 \cdot h^{-1} \cdot Pa^{-1}$) (Javanbakht et al., 2021). The procedure involved sealing the films onto the opening head of glass vessels (2.5 cm diameters) using silicone grease containing distilled water (15 mL). The vessels were then placed in desiccators filled with silica gel (RH gradient equal to 100 %) at room temperature. Weight loss resulting from the water vapor dilution passing over the wide-open film area (4.9 cm²) was recorded at different intervals. WVP was calculated using Eq. (3) after achieving steady-state conditions that took approximately 2 h A four-digit balance was also used to record eight weight measurements every hour.

$$WVP = \frac{d \times S}{\Delta P \times A} \tag{3}$$

where *S* is the slope of the weight loss vs. time (g·h⁻¹), *d* is the film thickness (m), *A* is the area of exposed film (m²). ΔP is the differential of water vapor pressure across the film ($\Delta P = 2.33 \times 10^3$ Pa, at ambient temperature, assuming that the RH on the silica gel is negligible).

2.4. Cell culture

Human skin fibroblast cells known as HFF-1 were obtained from the Pasteur Institute of Iran located in Tehran. These cells were cultured in Dulbeccom modified Eagle medium (DMEM). The DMEM consisted of a high glucose formulation, Gibco BRL, and contained 100 mg/mL streptomycin, 100 units/mL penicillin, and 10 % (v/v) fetal bovine serum. The cells were then triplicated into 96-well plates at a density of 1×10^4 cells/well. They were incubated at 37 °C for 24–48 h in an incubator that contained 5 % CO2. The cells were used for tests when they obtained 80 % confluence at the logarithmic growing phase.

2.5. Cell viability assay

The MTT assay was considered to determine the cytotoxicity of hydrogel films. Following sterilization with 70 % ethanol for 5 min, the films were washed twice with pH 7.4 (PBS) before being immersed in a fresh culture medium. HFF-1 cells were cultured in triplicate at a density of 104 cells per well into 96-well plates, both with and without samples. The addition of MTT solution (5 mg mL⁻¹) formed formazan crystals, which were solubilized with fresh culture medium after 4 h of

incubation. DMSO was added to dissolve the resulting MTT formazan residue, and the absorbance of solubilized formazan was read at 570 nm using a multi-well plate reader (Quant Bio-Tek Instruments, Winooski, VT, USA) after 30 min. Cell viability was determined using Eq. (4).

Cell viability (%) =
$$\frac{\text{Mean absorbance of each group}}{\text{Mean absorbance of control group}} \times 100$$
 (4)

2.6. Cellular uptake study

HFF-1 cells were seeded (3 \times 10⁵ cells per well density) in six-well plates and incubated overnight. They were treated with O-Alg/Ag-MOF/BX hydrogel for a desired time. Then, the cells were collected and washed three times with PBS, and cellular uptake images were captured using fluorescent microscopy (Cytation 5, Cell Imaging Multimode Reader, Biotek, USA).

2.7. Hemolysis rate assay

The hemolysis assay was conducted by making modifications to the previously reported approach (Kazeminava et al., 2022). Centrifugation was initially utilized to separate the plasma, which contained stable fresh human blood. The resulting pellets, consisting of human red blood cells, underwent three rinses with PBS to eliminate lysed hemoglobin at pH 7.4. These pellets were placed in a 10-fold diluted PBS solution and mixed with 1 mL of PBS-containing hydrogels. Subsequently, they were incubated for 1 h at 37 °C. DI water was employed to achieve 100 % hemolysis for the positive control, while a PBS solution served as the negative control with 0 % hemolysis. After incubation, the samples were centrifuged at 3500 rpm (1370 \times g) for 10 min. The absorbance of the supernatant in the 96-well plates was determined with a spectrophotometer at 545 nm. The hemolysis rate was calculated using Eq. (6).

Hemolysis Rate (%) =
$$\frac{(Abs \ sample \ -- Abs \ PBS)}{(Abs \ water \ -- Abs \ PBS)} \times 100$$
 (6)

2.8. Blood clotting

The blood clotting test was conducted according to the reported procedures (Mehrabani et al., 2018). Initially, the 12-well plate was filled with film samples measuring 10 mm in diameter. The plate was incubated at 37 °C for 15 min. Subsequently, stabilized blood (200 μL) was carefully applied to both the films and the control group. The blood clotting process was initiated by adding CaCl $_2$ solution (0.2 M) to the blood samples (40 μL). After an incubation of 15 min at 37 °C, the red blood cells became trapped within the clot. To induce hemolysis of the blood cells, 6 mL of deionized water was added to each well. Following gentle shaking for 2 min, 2 mL aliquot of the medium was withdrawn and centrifuged at 1500 rpm (252 \times g) for 2 min. The absorbance of the supernatant was read using an ELISA reader (BioTech) at a wavelength of 540 nm. The blood clotting index (BCI) was determined using Eq. (5) for the given samples.

$$BCI = \frac{ODSample}{ODControl} \tag{5}$$

where $\mathrm{OD}_{\text{sample}}$ and $\mathrm{OD}_{\text{Control}}$ were absorbances of blood in contact with and without samples, respectively.

2.9. Antimicrobial activity of films

The agar disc diffusion method was utilized to evaluate the antimicrobial effectiveness (Kazeminava et al., 2022). To examine the antibacterial properties, the prepared films underwent testing against *S. aureus* (ATCC 25,923) and *E. coli* (ATCC 25,922) bacteria. The bacterial strains were adjusted to a concentration of 0.5 McFarland standard and subsequently treated on the agar plate surface. Subsequently, all

films with a diameter of 8 mm were as eptically cut and placed onto agar plates, which were then incubated at $37\,^\circ\text{C}.$ The resulting zones of inhibition were measured after a period of 18--24~h

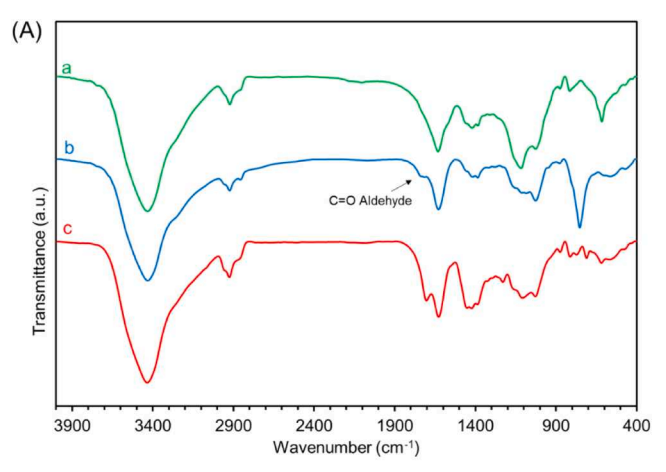
2.10. Bacterial barrier assay of films

To assess the films' capacity to inhibit bacterial growth, E. coli and S. aureus were employed as test microorganisms, and the quantity of bacterial colonies on the agar medium was examined. Initially, the mixtures were sterilized using ultraviolet light. Subsequently, hydrogel films were applied onto the nutrient agar through a spray-by-spray technique, resulting in a film thickness of about 1 mm. The hydrogel film surface was then plated with S. aureus at a 5 \times 10⁶ CFU mL⁻¹ density (Husain et al., 1983). A control group was established for comparison by placing the same quantity of S. aureus onto the nutrient agar without the film covering. After an incubation period of 6, 12, and 24 h at 37 °C, the plates were further incubated after removing films under identical conditions for an additional 48 h Each incubation time point consisted of three samples, and the number of colonies was documented. To evaluate the hydrogel films' effectiveness against both gram-positive and negative bacteria, the same procedure was followed using E. coli at the same density instead of S. aureus.

3. Result and discussion

3.1. Characterization of the synthesized hydrogel

Fig. 2A shows the FT-IR spectra of Alg, O-Alg, and O-Alg/Ag-MOF/BX hydrogel. By comparing the FT-IR spectrum of Alg and O-Alg, a



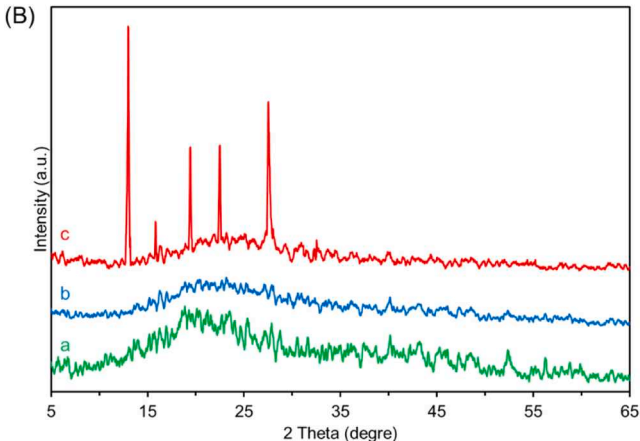


Fig. 2. A) FT-IR spectra of the Alg (a), O-Alg (b), and O-Alg/Ag-MOF/BX (c). B) XRD patterns of Alg (a), O-Alg (b) and O-Alg/Ag-MOF/BX (c).

shoulder peak at 1735 cm⁻¹ corresponding to the C = O aldehyde stretching vibration confirms the oxidation of Alg (Mohammadzadeh et al., 2024). Also, the changes observed in 1400 cm⁻¹ and 1650 cm⁻¹ areas after the construction of O-Alg/Ag-MOF/BX can verify the creation of Ag-MOF nanoparticles in the hydrogel network (Guo et al., 2017). Fig. 2B shows the XRD pattern of Alg and O-Alg/Ag-MOF/BX hydrogel. In the XRD pattern of Alg, two weak and broad peaks can be seen at 2θ around 14.0° and 20.9°, indicating the amorphous structure of this biopolymer (Zheng et al., 2016). The XRD pattern of O-Alg is similar to the Alg, which confirmed that the structure of Alg was perceived during its partial oxidation. However, in the XRD pattern of O-Alg/Ag-MOF/BX hydrogel, in addition to the broad peak related to Alg biopolymer, sharp peaks were observed at 2θ about 13.0° , 15.8° , 19.4° , 22.4° and 27.6° , which can be related to the formation of the Ag-MOF (Guo et al., 2017). These results confirm the successful in-situ creation of Ag-MOF toward the construction of O-Alg/Ag-MOF/BX hydrogel film.

The gelation times of the O-Alg/Ag-MOF/BX hydrogel were systematically evaluated to assess its rapid-forming behavior, which is crucial for effective wound dressing applications. The gelation time can be finely tuned by adjusting the ratio of ATPA/BX to O-Alg/Ag(OAc). Notably, increasing the volume ratio (spraying cycles) of ATPA/BX to O-Alg/Ag(OAc) from 1:1 to 3:1 resulted in a significant reduction in gelation time from 30 s to just 5 s. This rapid gelation is essential for creating efficient spray films that can quickly adhere to wounds upon application. All observed gelation times imitate established criteria for rapidly formed spray films (Du et al., 2020; Li et al., 2024), which enhances their applicability in emergency settings where time is critical. The direct spraying method employed for O-Alg/Ag(OAc) and ATPA/BX facilitates the formation of a double cross-linked network within the hydrogel through multiple bonding mechanisms, including boronic ester linkages, electrostatic interactions, and Schiff base formations. This multifaceted cross-linking not only contributes to the structural integrity

of the hydrogel but also allows for the rapid in-situ synthesis of Ag-MOF nanoparticles. As illustrated in Figure S2, this unique formulation process positions the O-Alg/Ag-MOF/BX hydrogel as an ideal candidate for use as a spray-on wound dressing. Its ability to be rapidly applied to mass wounds addresses one of the significant limitations associated with conventional hydrogels, which often require longer application times and may not provide immediate protection against infection.

Hydrogel morphology is a critical characteristic influencing its biomedical applications, particularly in wound healing. As shown in Fig. 3, SEM images reveal distinct morphological differences between Alg/BX and O-Alg/Ag-MOF/BX hydrogel films. The Alg/BX hydrogel film exhibits a uniform surface morphology, which is beneficial for consistent application but may limit its interaction with biological tissues. In contrast, high-magnification SEM images of the O-Alg/Ag-MOF/ BX film reveal a wrinkled morphology with numerous pores in its inner regions. This unique structure likely arises from the cross-linking of Alg with BX and is essential for enhancing fluid absorption and gas exchange at the wound site. The incorporation of Ag(OAc) and ATPA into the O-Alg matrix resulted in observable crystalline structures on the film surface, indicative of Ag-MOF formation. These crystalline features are significant as they not only contribute to the mechanical stability of the hydrogel but also enhance its antibacterial properties through sustained silver ion release. Additionally, AFM images corroborate these findings by demonstrating a rougher morphology for O-Alg/Ag-MOF/BX compared to Alg/BX. This increased roughness is advantageous as it improves adhesion to biological surfaces, such as skin, facilitating better integration and functionality as a wound dressing.

Fig. 4 displays the elemental mapping images and EDX spectrum of O-Alg/Ag-MOF/BX hydrogel film. They can confirm the formation of O-Alg/Ag-MOF/BX by stating that only B, C, O, N, Na, and Ag elements are present and prove the purity and proper distribution of elements on the surface of the constructed film. The presence of silver is particularly

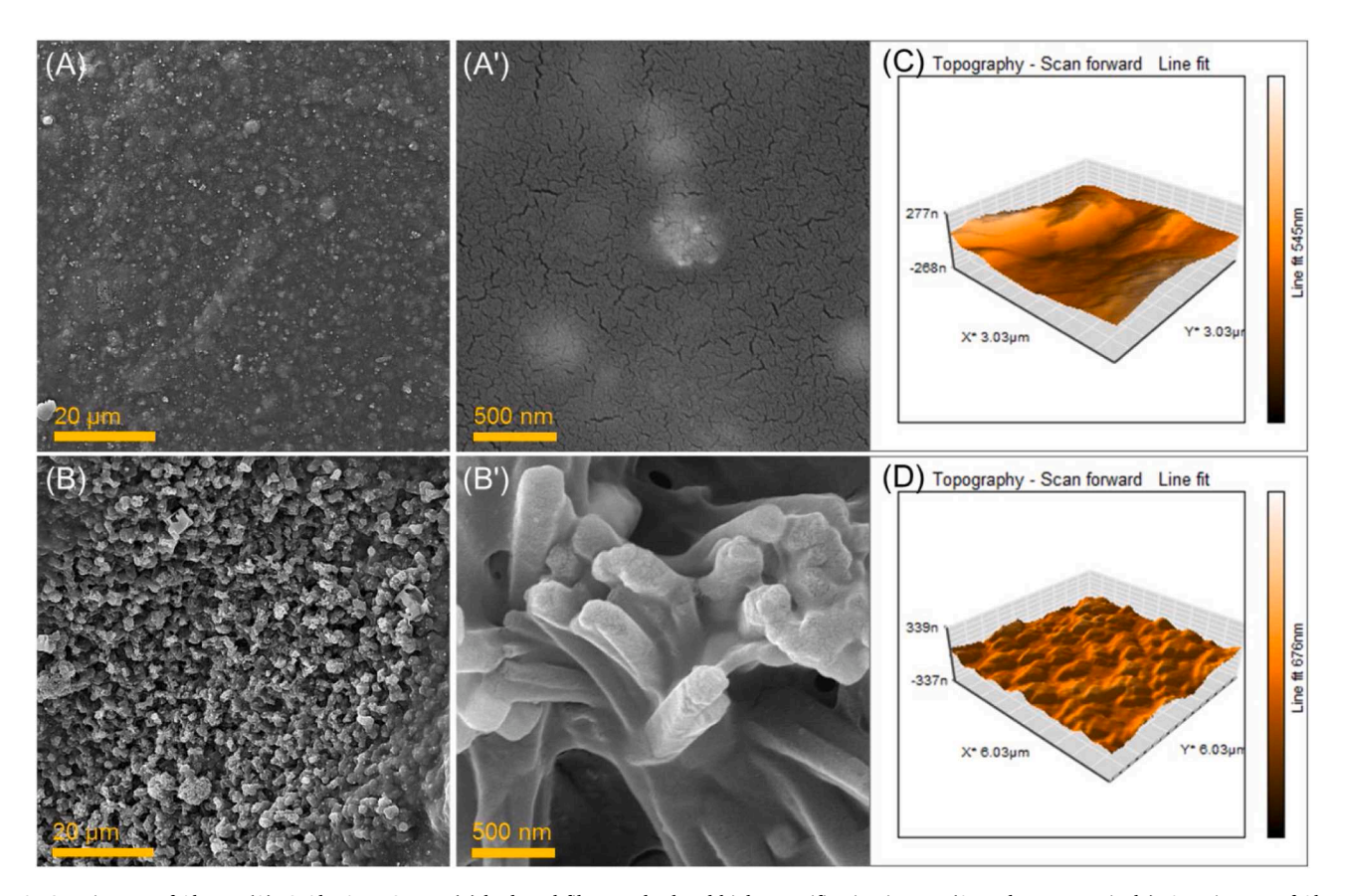


Fig. 3. SEM images of Alg/BX (A), O-Alg/Ag-MOF/BX (B) hydrogel films, and related high magnification images (A' and B', respectively). AFM images of Alg/BX (A), O-Alg/Ag-MOF/BX (B) hydrogel films.

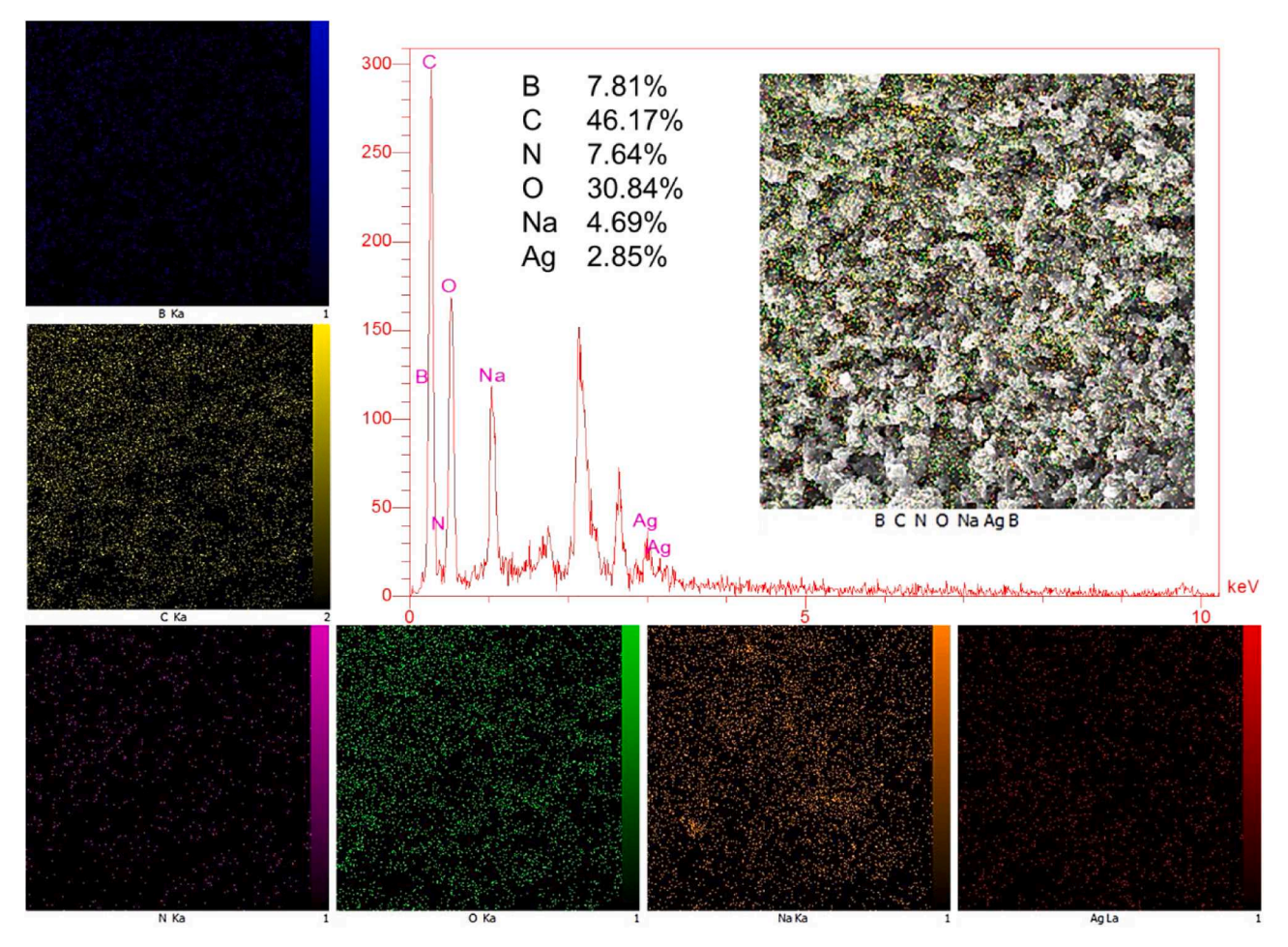


Fig. 4. Elemental mapping images and EDX spectrum of O-Alg/Ag-MOF/BX hydrogel film.

noteworthy as it correlates with the hydrogel's antibacterial properties, while boron contributes to its cross-linking efficiency. This homogeneous elemental distribution enhances the mechanical stability and functional efficacy of the hydrogel, making it suitable for use as a wound dressing.

The diagrams in Fig. 5 display the tensile strength, elongation at

break, and WVP of the Alg/BX and O-Alg/Ag-MOF/BX hydrogel films. Incorporating Ag-MOF nanoparticles into the Alg network enhanced the hydrogel film's tensile strength, likely due to their cross-linking properties (Fig. 5A). Additionally, the elongation at break values of the films was raised by the incorporation of Ag-MOF, indicating improved flexibility (Fig. 5B). These results demonstrate that Ag-MOF nanoparticles

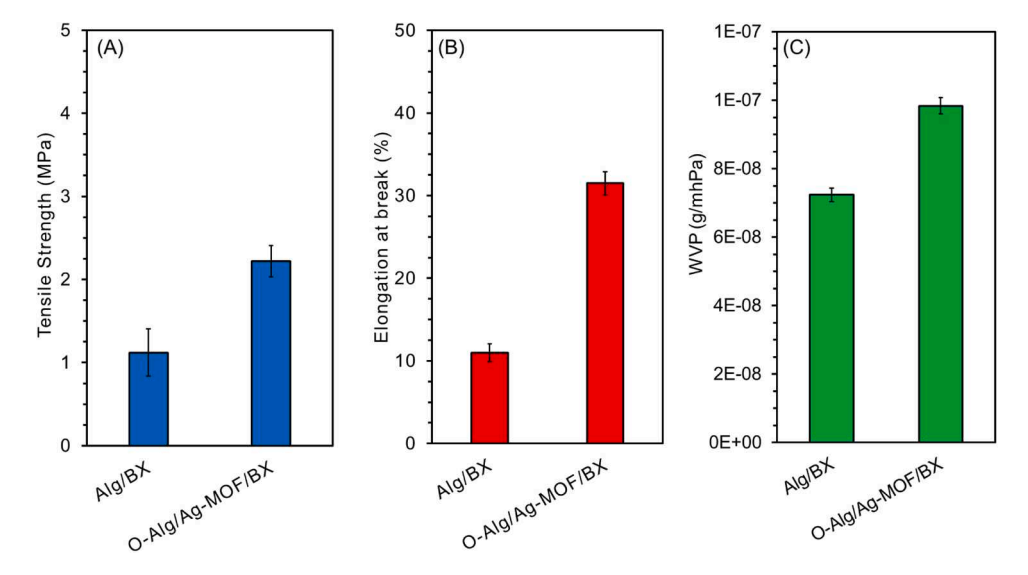


Fig. 5. Diagrams represent (A) tensile strength, (B) elongation at break, and (C) WVP of the Alg/BX and O-Alg/Ag-MOF/BX hydrogel films (the average of 3 experiments was reported).

contribute to higher elasticity in the hydrogel network by forming Schiff base imine, a dynamic bond. Previous studies have shown that the dynamic Schiff base and boronic ester bonds formed during cross-linking significantly improve the flexibility and durability of hydrogels, making them suitable for irregular wound coverage (Zhang et al., 2024). On the other hand, the mechanical characteristics of the nanocomposite films could withstand pressures exerted on diverse body parts or wounds (Yadollahi et al., 2014; Rakhshaei & Namazi, 2017).

Additionally, the impact of Ag-MOF nanoparticles on the WVP of hydrogel films is depicted in Fig. 5C. The experimental results indicate an increase in WVP values after including in-situ formed Ag-MOF nanoparticles within the Alg network. This could be attributed to forming a porous region surrounding the nanoparticles within the polymer matrix, resulting in enhanced permeability of the hydrogel film. The increased permeability is particularly advantageous for wound dressing applications, as it allows for optimal moisture management at the wound site, promoting a conducive environment for healing while preventing excessive moisture loss. Maintaining appropriate hydration levels is essential for effective wound healing, as it supports cellular activities and reduces scab formation, which can impede recovery. Moreover, this finding aligns with previous studies that have reported similar enhancements in WVP when incorporating porous materials into hydrogels (Park et al., 1993). The ability to regulate moisture levels effectively positions the O-Alg/Ag-MOF/BX hydrogel as a promising candidate for advanced wound dressings, particularly in scenarios involving large or irregularly shaped wounds where moisture management is critical.

Fig. 6 illustrates the behavior of the hydrogel films in a PBS solution

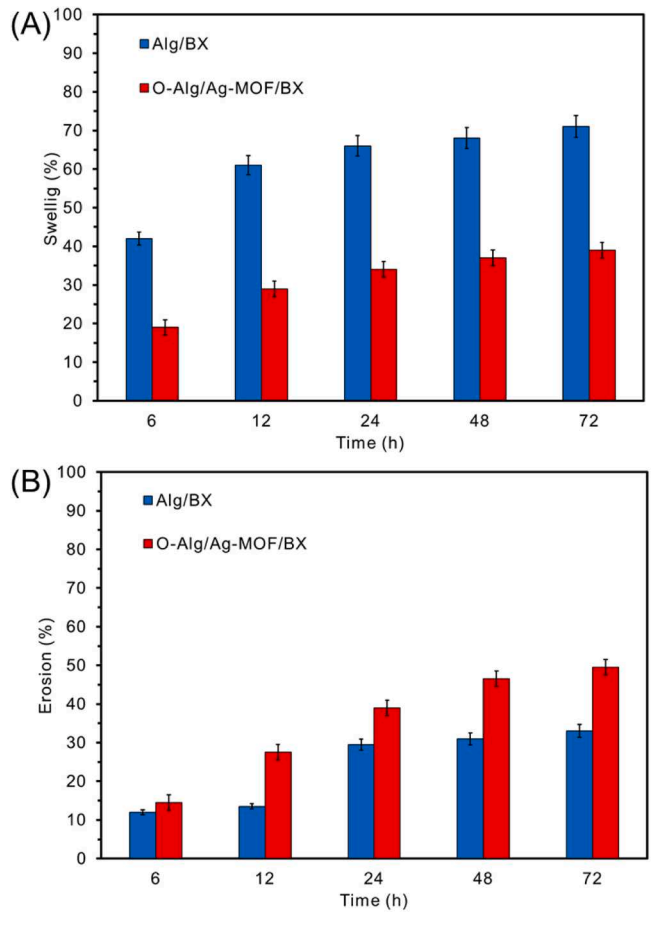


Fig. 6. The swelling and erosion diagrams for the Alg/BX, O-Alg/Ag-MOF/BX hydrogel films at $37~^{\circ}$ C in PBS (pH 7.4) (the average of three measurements was reported).

(pH 7.4) at 37 °C. The films demonstrated an increased swelling ratio over time, indicating a time-dependent swelling behavior. Incorporating Ag-MOF nanoparticles into the Alg biopolymeric network diminished the swelling ratio, potentially attributed to the cross-linking ability of these nanoparticles (Fig. 6A). This reduction can be attributed to the cross-linking ability of Ag-MOF nanoparticles, which likely creates a more compact structure that limits excessive water absorption. Additionally, the erosion data revealed a weight loss of approximately 50 % after 72 h, further increased by the Ag-MOF nanoparticles (Fig. 6B). This weight loss can be due to the degradation of Ag-MOF nanoparticles and the subsequent release of Ag⁺ from the biopolymeric network. The results confirm that the prepared O-Alg/Ag-MOF/BX hydrogel film has degradation capabilities in PBS media (Bari et al., 2016). This controlled degradation not only enhances antibacterial efficacy through silver ion release but also supports tissue regeneration by providing a conducive environment for healing.

3.2. Hemolysis and blood clotting studies

In the context of hemostatic agents, the evaluation of hemocompatibility is crucial and can be accomplished through hemolysis testing. The interaction between erythrocytes (red blood cells) and hydrogel in contact with blood is vital in determining the release of hemoglobin. Fig. 7A illustrates the hemolysis ratio observed in the prepared hydrogel films. Despite including Ag-MOF nanoparticles in the Alg hydrogel film formulation, the hemolysis ratio remained below 4 %. This low percentage indicates excellent hemocompatibility and is comparable to other materials reported in the literature for hemostatic applications (Kazeminava et al., 2022; Eivazzadeh-Keihan et al., 2021). Such favorable hemocompatibility is critical for wound dressings as it

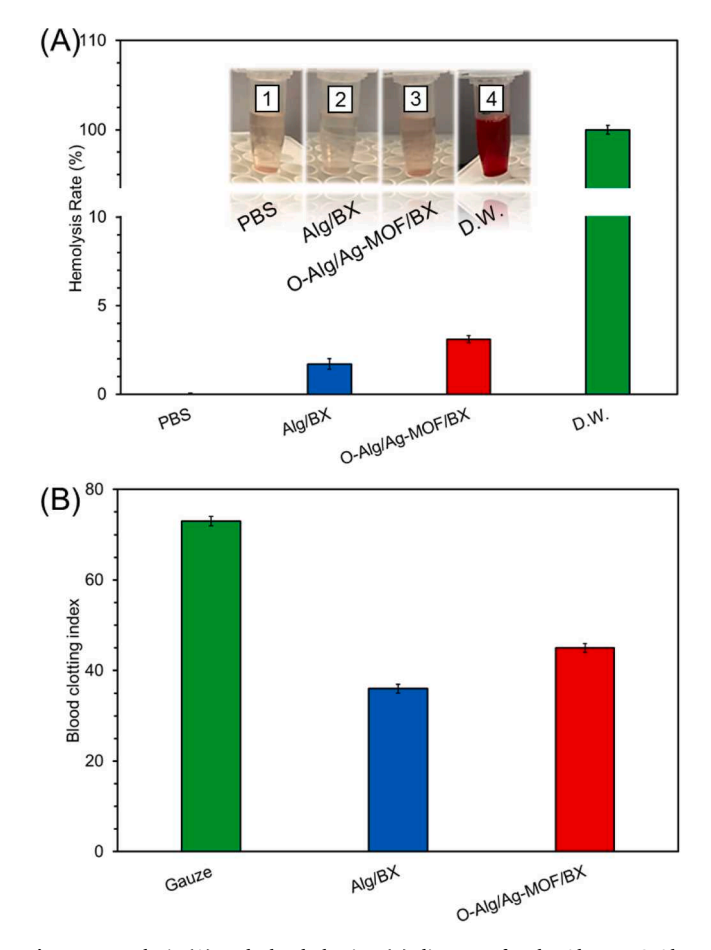


Fig. 7. Hemolysis (A) and Blood clotting (B) diagrams for the Alg/BX, O-Alg/Ag-MOF/BX hydrogel films (the average of three measurements was reported).

minimizes adverse reactions when in contact with blood, thereby enhancing patient safety and comfort.

Another significant aspect of wound dressings made from biomaterials is their ability to promote blood clotting. The findings of the research on blood clotting are illustrated in Fig. 7B. Based on the results, the nanocomposite films containing Ag-MOF nanoparticles exhibit a slight improvement in blood clotting capability. However, the blood clotting ability of the O-Alg/Ag-MOF/BX hydrogel film is comparable to that of commercially available gauze (Mehrabani et al., 2018). This similarity may be attributed to the inherent bioactivity of polysaccharide-based platforms, which are known to facilitate coagulation processes. These findings underscore the potential of the O-Alg/Ag-MOF/BX hydrogel film as an effective wound dressing material with notable hemostatic properties. The combination of excellent hemocompatibility and efficient blood clotting capability positions this hydrogel as a promising candidate for clinical applications in managing wounds, particularly in scenarios where rapid hemostatic action is required.

3.3. Cytotoxicity study

MTT test was conducted to assess the cytotoxicity of prepared hydrogel films towards HFF-1 cell lines. The remaining cell viability over ~80 %, even after 5-day incubation, revealed the good cytocompatibility of prepared films (Fig. 8A). Alternatively, the hydrogel film cytotoxicity was slightly reduced by incorporating Ag-MOF and prolonged treatment time. The desired cytocompatibility of the O-Alg/ Ag-MOF/BX can be due to the non-cytotoxicity nature of Alg reported in the literature (Urzedo et al., 2020). In addition, due to the suitable photoluminescent (PL) properties of O-Alg/Ag-MOF/BX (excitation: 320 nm, emission: 430 nm, Figure S3) initiated from the fluorescent features of amine-functionalized Ag-MOF (Dong et al., 2019), it has an outstanding possibility to be utilized for cell imaging study. As seen in the cellular uptake images (Fig. 8B-D), the cell internalization of O-Alg/Ag-MOF/BX was detected in HFF-1 cells, suggesting that fluorescent ATPA ligand released through the erosion of O-Alg/Ag-MOF/BX was transported into the cells, Fig. 6B. Moreover, the intensity of blue fluorescence was enhanced over time up to 4 h; accordingly, the intracellular ATPA concentrations and the cell cytotoxicity were raised,

which is in accordance with MTT outcomes. Nevertheless, this level of cytocompatibility is essential for any wound dressing intended for clinical use, as it suggests that the hydrogel can promote cellular proliferation while minimizing adverse reactions (Gupta et al., 2019). Similar to other hydrogels reported in the literature (Mahajan et al., 2024; Virzì et al., 2024), the present formulation demonstrates superior biocompatibility, positioning it as a promising candidate for wound healing applications.

3.4. Antibacterial and bacterial barrier assays of the hydrogel films

Barrier protection is a productive technique for safeguarding wounds and the surrounding areas (Stephen-Haynes, 2014). Materials such as skin act as barriers, preventing water loss and shielding internal organs from the external environment (Schuren et al., 2005; Fan et al., 2014). In large-scale disasters, warfare, and road accidents, numerous injuries arise, necessitating prompt dressing to evade severe consequences. Dressings employed in these circumstances should promptly form a protective film to manage a high volume of casualties. With this objective in mind, a simple-forming O-Alg/Ag-MOF/BX hydrogel film was formulated, eliminating the need for additional fixtures on the skin (Figure S2). The rapid-forming capability of these hydrogels allows them to create a film through spraying, which offers a practical and straightforward approach to addressing irregular and mass wounds.

To evaluate the effectiveness of the O-Alg/Ag-MOF/BX hydrogel film in protecting wounds, a film was created by spraying O-Alg/Ag(OAc) and ATPA/BX onto agar (Fig. 9, film covered). The films were then treated with *S. aureus* and *E. coli* and incubated at specific intervals. The agar plates were further incubated after removing films with colonies. Removing the film did not cause any damage to the agar, indicating that the O-Alg/Ag-MOF/BX hydrogel films could prevent secondary injury when removing the dressing from wounds (Fig. 9, 6h). Unlike the control group, no colonies of *S. aureus* and *E. coli* were detected on the agar surfaces covered with O-Alg/Ag-MOF/BX hydrogel film at 6 and 12 h; however, some colony found on the agar plate after 24 h (Fig. 9). These findings demonstrate that the O-Alg/Ag-MOF/BX hydrogel film effectively acts as a barrier against *S. aureus* and *E. coli* for 12 h Typically, the effective duration for debridement in a clinical environment is 6 h (Crowley et al., 2007). The present film, O-Alg/Ag-MOF/BX, fulfills the

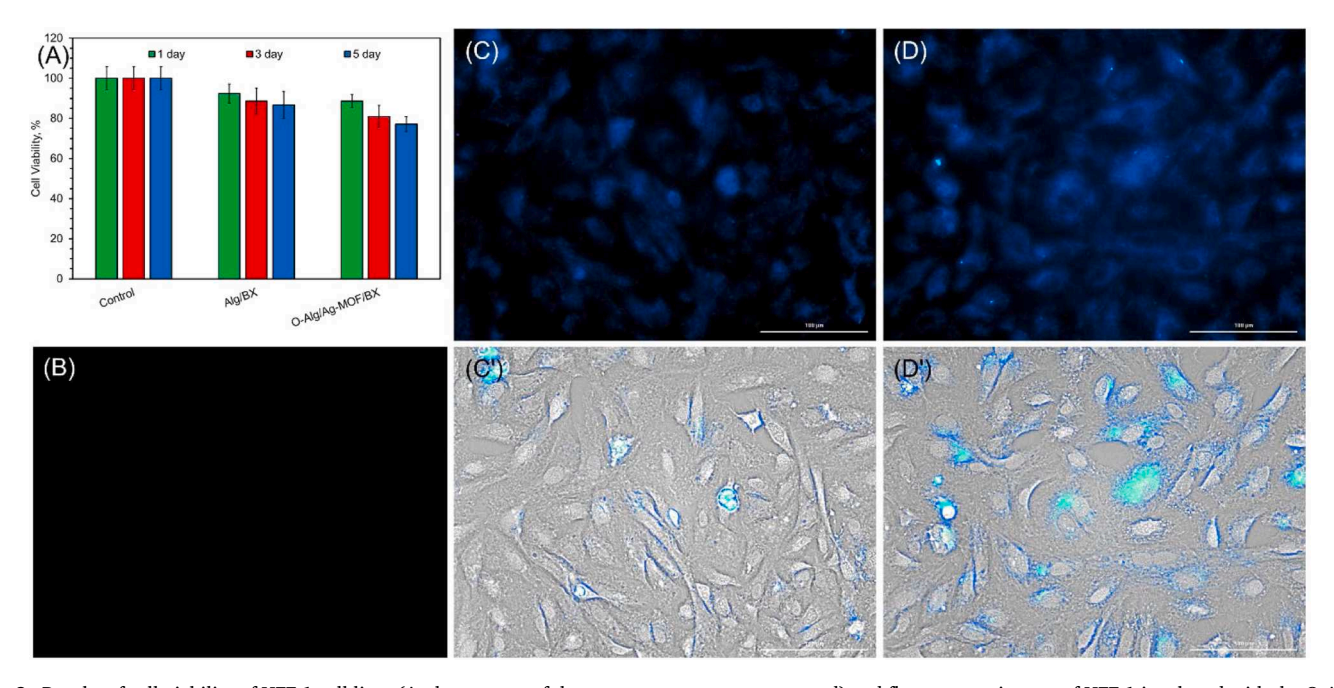


Fig. 8. Results of cell viability of HFF-1 cell lines (A, the average of three measurements was reported) and fluorescence images of HFF-1 incubated with the O-Alg/Ag-MOF/BX at 37 °C for different incubated time, 0 h (B), 2 h (C), and 4 h (D). The related overlay images are shown in C' and D'. Scale bar: 10 μm.

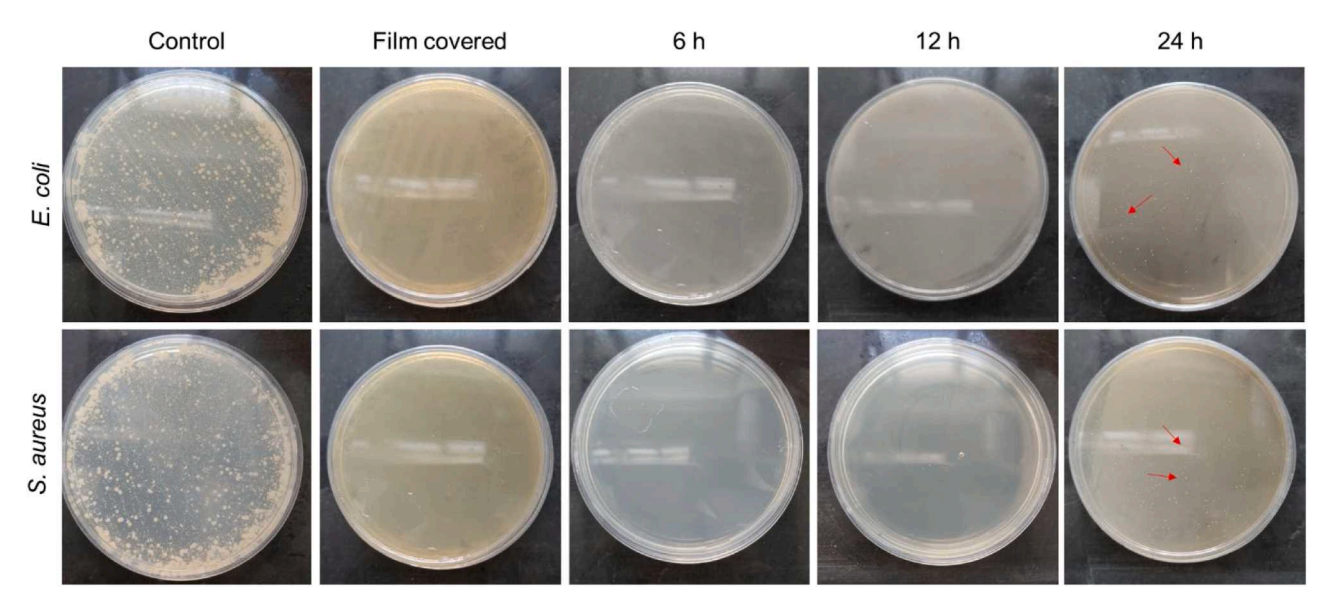


Fig. 9. Photographs of E. coli and S. aureus colonies formed on agar covered with O-Alg/Ag-MOF/BX hydrogel film after 6, 12, and 24 h, and agar with no film covering was used as a control.

requirement for safeguarding wounds before debridement. This sustained antibacterial activity is critical in clinical scenarios where prolonged protection is necessary to prevent infection during initial healing phases. Furthermore, this platform offers extended protection for injuries in which immediate medical intervention is not readily accessible. The combination of physical barrier properties and inherent antibacterial action makes this hydrogel particularly advantageous for use in emergency medical situations involving large or irregularly shaped wounds. Additionally, when compared with traditional dressings, medical gauze covered on agar for 6 h showed significant bacterial growth (Du et al., 2020). This implies that the O-Alg/Ag-MOF/BX hydrogel film, functioning as a dressing, can significantly enhance infection prevention.

Additionally, the outcomes of evaluating the inhibitory action of the prepared hydrogel films against S. aureus and E. coli bacteria are presented in Table 1. The Alg/BX (control) did not display any antibacterial behavior; however, the O-Alg/Ag-MOF/BX hydrogel film exhibited inhibition zones against both types of bacteria (1.3 \pm 0.1 cm). The incorporation of Ag-MOF nanoparticles in the Alg hydrogel made significant antibacterial activity. Notably, it was observed that the O-Alg/Ag-MOF/BX hydrogel film possessed similar efficacy against both grampositive and negative bacteria. This is attributed to the availability of Ag-MOFs on the film surface, which enables direct contact with bacterial cells and enhances the antibacterial property through excellent toxicity. In simpler terms, MOFs can serve as a reservoir of metal ions, including

silver (Ag⁺), and the gradual release of these ions due to framework destruction ensures sustainable antibacterial activity. This finding is consistent with previous reports that highlight the effectiveness of silver-based materials in preventing bacterial growth (Berchel et al., 2011). The sustained release of silver ions from Ag-MOF within the hydrogel matrix is likely responsible for this prolonged antibacterial effect, which is crucial for managing infections in traumatic wounds (Wyszogrodzka et al., 2016). Furthermore, the organic linker used to construct the framework may possess inherent antimicrobial activity. leading to a synergistic effect (Wyszogrodzka et al., 2016). Notably, the antibacterial capacity of silver-based MOFs primarily depends on the controlled release of Ag+ ions (Berchel et al., 2011). However, the effectiveness of antibacterial properties is directly proportional to the amount of Ag+ ions released (Lu et al., 2014). Given that microbial adhesion typically leads to bacterial colonization and biofilm formation, strategies to prevent microorganism attachment offer promising solutions for mitigating film fouling (Banerjee et al., 2011). Therefore, considering the antibacterial activity and bacterial barrier capability, spray-filming properties, and ability to form a protective film, the O-Alg/Ag-MOF/BX hydrogel film proves to be an effective barrier for wounds. This flexible film enables prompt management of numerous wounds, protects against further invasion, and offers safer conditions and additional time for transferring the injured.

Table 1Antibacterial inhibition zones (cm) of the hydrogel films.

Bacteria Photographs of the inhibition zone		E. coli	S. aureus
1	Alg/BX	0.8 ± 0.1	0.8 ± 0.1
2	O-Alg/Ag-MOF/BX	1.3 ± 0.1	1.3 ± 0.1
2''	O-Alg/Ag-MOF/BX	1.4 ± 0.1	1.3 ± 0.1

Note: The reported values are a mean \pm SD of three determinations.

4. Conclusions

The O-Alg/Ag-MOF/BX hydrogel was successfully synthesized through a cross-linking reaction involving O-Alg, BX, and aminefunctionalized Ag-MOF. The resulting hydrogels exhibited remarkable spray-filming capabilities, attributed to the rapid formation of Schiff base and boronic ester bonds, which provided effective and long-lasting wound protection. The in-situ formation of the antibacterial Ag-MOF during hydrogel preparation enhanced both the gelation rate and stability of the hydrogel by establishing a double cross-linked network. This innovation resulted in rapid spray-filming performance, making the O-Alg/Ag-MOF/BX hydrogel particularly suitable for treating irregular and mass wounds. Furthermore, the hydrogel demonstrated significant antibacterial activity against common pathogens, including S. aureus and E. coli, maintaining its barrier capability for up to 12 h Importantly. it exhibited good cytocompatibility with HFF-1 cells, indicating its safety for potential clinical applications. Given its design for external use, concerns regarding systemic penetration and accumulation of its nanosized components are minimal; any absorption would be localized at the application site, reducing risks associated with internal accumulation. To enhance the practicality and applicability of this hydrogel in real-world scenarios, particularly in emergency situations involving large wound areas, future research could focus on (I) Utilizing a dualchamber spray applicator for simultaneous application of both solutions. (II) Optimizing material concentrations to further reduce gelation time. (III) Investigating the possibility of combining some components into a single solution without compromising performance. These additional studies could significantly improve the efficiency and ease of use of this hydrogel in managing and protecting wounds resulting from road accidents, disasters, and war injuries.

CRediT authorship contribution statement

Siamak Javanbakht: Writing – original draft, Visualization, Validation, Software, Project administration, Methodology, Investigation, Formal analysis, Data curation, Conceptualization. **Reza Mohammadi:** Writing – review & editing, Validation, Supervision, Resources.

Declaration of competing interest

The authors declare that they have no known competing financial interests or personal relationships that could have appeared to influence the work reported in this paper.

Acknowledgments

This research was supported with a research grant of the University of Tabriz (number SAD/2389–14020820).

Supplementary materials

Supplementary material associated with this article can be found, in the online version, at doi:10.1016/j.carpta.2024.100629.

Data availability

The data that support the findings of this study are available from the corresponding author, upon reasonable request.

References

- Balakrishnan, B., Joshi, N., Jayakrishnan, A., & Banerjee, R. (2014). Self-crosslinked oxidized alginate/gelatin hydrogel as injectable, adhesive biomimetic scaffolds for cartilage regeneration. Acta biomaterialia, 10(8), 3650–3663.
- Banerjee, I., Pangule, R. C., & Kane, R. S. (2011). Antifouling coatings: Recent developments in the design of surfaces that prevent fouling by proteins, bacteria, and marine organisms. Advanced materials, 23(6), 690–718.

- Bari, S. S., Chatterjee, A., & Mishra, S. (2016). Biodegradable polymer nanocomposites: An overview. *Polymer Reviews*, 56(2), 287–328.
- Berchel, M., Le Gall, T., Denis, C., Le Hir, S., Quentel, F., Elleouet, C., Montier, T., Rueff, J.-M., Salaün, J.-Y., & Haelters, J.-P. (2011). A silver-based metal-organic framework material as a 'reservoir' of bactericidal metal ions. *New Journal of Chemistry*, 35(5), 1000–1003.
- Cha, G. D., Lee, W. H., Sunwoo, S.-H., Kang, D., Kang, T., Cho, K. W., Kim, M., Park, O. K., Jung, D., & Lee, J. (2022). Multifunctional injectable hydrogel for in vivo diagnostic and therapeutic applications. ACS nano, 16(1), 554–567.
- Chen, T., Chen, Y., Rehman, H. U., Chen, Z., Yang, Z., Wang, M., Li, H., & Liu, H. (2018). Ultratough, self-healing, and tissue-adhesive hydrogel for wound dressing. ACS Applied Materials & Interfaces, 10(39), 33523–33531.
- Crowley, D., Kanakaris, N., & Giannoudis, P. (2007). Debridement and wound closure of open fractures: The impact of the time factor on infection rates. *Injury*, *38*(8), 879–889
- da Silva, L. P., Reis, R. L., Correlo, V. M., & Marques, A. P. (2019). Hydrogel-based strategies to advance therapies for chronic skin wounds. *Annual Review of Biomedical Engineering*, 21(1), 145–169.
- Dong, J., Zhao, D., Lu, Y., & Sun, W.-Y. (2019). Photoluminescent metal-organic frameworks and their application for sensing biomolecules. *Journal of Materials Chemistry A*, 7(40), 22744–22767.
- Du, Y., Li, L., Peng, H., Zheng, H., Cao, S., Lv, G., Yang, A., Li, H., & Liu, T. (2020). A spray-filming self-healing hydrogel fabricated from modified sodium alginate and gelatin as a bacterial Barrier. *Macromolecular Bioscience*, 20(2), Article 1900303.
- Eivazzadeh-Keihan, R., Khalili, F., Khosropour, N., Aliabadi, H. A. M., Radinekiyan, F., Sukhtezari, S., Maleki, A., Madanchi, H., Hamblin, M. R., & Mahdavi, M. (2021). Hybrid bionanocomposite containing magnesium hydroxide nanoparticles embedded in a carboxymethyl cellulose hydrogel plus silk fibroin as a scaffold for wound dressing applications. ACS Applied Materials & Interfaces, 13(29), 33840–33849.
- Fan, Z., Liu, B., Wang, J., Zhang, S., Lin, Q., Gong, P., Ma, L., & Yang, S. (2014). A novel wound dressing based on Ag/graphene polymer hydrogel: Effectively kill bacteria and accelerate wound healing. Advanced Functional Materials, 24(25), 3933–3943.
- Guo, H., Zhang, Y., Zheng, Z., Lin, H., & Zhang, Y. (2017). Facile one-pot fabrication of Ag@ MOF (Ag) nanocomposites for highly selective detection of 2, 4, 6-trinitrophenol in aqueous phase. *Talanta*, 170, 146–151.
- Gupta, A., Kowalczuk, M., Heaselgrave, W., Britland, S. T., Martin, C., & Radecka, I. (2019). The production and application of hydrogels for wound management: A review. European Polymer Journal, 111, 134–151.
- Hachimi Alaoui, C., & Fatimi, A. (2023). A 20-year patent review and innovation trends on hydrogel-based coatings used for medical device biofabrication. *Journal of Biomaterials Science, Polymer Edition*, 34(9), 1255–1273.
- Hong, L., Liu, L., Zhang, Z., Song, J., Li, S., Chen, K., Gao, G., & Wang, Y. (2022). Tough and self-healing hydrogels based on transient crosslinking by nanoparticles. Soft Matter, 18(9), 1885–1895.
- Husain, M., Akhtar, M., & Akhtar, N. (1983). Report on evaluation of hydron film as burn wound dressing. Burns, 9(5), 330–334.
- Javanbakht, S., Nabi, M., Shadi, M., Amini, M. M., & Shaabani, A. (2021). Carboxymethyl cellulose/tetracycline@ UiO-66 nanocomposite hydrogel films as a potential antibacterial wound dressing. *International Journal of Biological Macromolecules*, 188, 811–819.
- Jeong, D., Jang, S. Y., Roh, S., Choi, J. H., Seo, I. J., Lee, J. H., Kim, J., Kwon, I., Jung, Y., & Hwang, J. (2024). Sprayable hydrogel with optical mRNA nanosensors for Real-Time monitoring and healing of diabetic wounds. *Chemical Engineering Journal*, Article 152711
- Kazeminava, F., Javanbakht, S., Nouri, M., Gholizadeh, P., Nezhad-Mokhtari, P., Ganbarov, K., Tanomand, A., & Kafil, H. S. (2022). Gentamicin-loaded chitosan/folic acid-based carbon quantum dots nanocomposite hydrogel films as potential antimicrobial wound dressing. *Journal of Biological Engineering*, 16(1), 1–13.
- Kesharwani, P., Bisht, A., Alexander, A., Dave, V., & Sharma, S. (2021). Biomedical applications of hydrogels in drug delivery system: An update. *Journal of Drug Delivery Science and Technology*, 66, Article 102914.
- Li, H., Wang, Y., Guo, L., Huang, L., Li, X., & Gao, W. (2024a). Polysaccharide hydrogels for diabetic wounds: Reasonable customization and regulatory mechanisms. *Chemical Engineering Journal*, Article 154143.
- Li, Q., Liu, K., Jiang, T., Ren, S., Kang, Y., Li, W., Yao, H., Yang, X., Dai, H., & Chen, Z. (2021a). Injectable and self-healing chitosan-based hydrogel with MOF-loaded α-lipoic acid promotes diabetic wound healing. *Materials Science and Engineering: C*, 131, Article 112519.
- Li, Q., Wen, J., Liu, C., Jia, Y., Wu, Y., Shan, Y., Qian, Z., & Liao, J. (2019). Graphenenanoparticle-based self-healing hydrogel in preventing postoperative recurrence of breast cancer. ACS Biomaterials Science & Engineering, 5(2), 768–779.
- Li, R., Chen, T., & Pan, X. (2021b). Metal-organic-framework-based materials for antimicrobial applications. ACS nano, 15(3), 3808–3848.
- Li, X., Lin, H., Yu, Y., Lu, Y., He, B., Liu, M., Zhuang, L., Xu, Y., & Li, W. (2024b). In situ rapid-formation sprayable hydrogels for challenging tissue injury management. Advanced Materials, Article 2400310.
- Lu, X., Ye, J., Zhang, D., Xie, R., Bogale, R. F., Sun, Y., Zhao, L., Zhao, Q., & Ning, G. (2014). Silver carboxylate metal–organic frameworks with highly antibacterial activity and biocompatibility. *Journal of inorganic biochemistry*, 138, 114–121.
- Mahajan, P., Nangare, S., Patil, A., Jain, P., & Zawar, L. (2024). Chia (Salvia hispanica L.) seed mucilage (a heteropolysaccharide) based antimicrobial hydrogel scaffold for wound healing: In vitro-in-vivo characterization. Carbohydrate Polymer Technologies and Applications, 7, Article 100432.
- Mansour, F. R., Abdelhameed, R. M., Hammad, S. F., Abdallah, I. A., Bedair, A., & Locatelli, M. (2024). A microcrystalline cellulose/metal-organic framework hybrid

- for enhanced ritonavir dispersive solid phase microextraction from human plasma. *Carbohydrate Polymer Technologies and Applications*, 7, Article 100453.
- Mehrabani, M. G., Karimian, R., Rakhshaei, R., Pakdel, F., Eslami, H., Fakhrzadeh, V., Rahimi, M., Salehi, R., & Kafil, H. S. (2018). Chitin/silk fibroin/TiO2 bionanocomposite as a biocompatible wound dressing bandage with strong antimicrobial activity. *Int J Biol Macromol*, 116, 966–976.
- Mo, C., Xiang, L., & Chen, Y. (2021). Advances in injectable and self-healing polysaccharide hydrogel based on the Schiff base reaction. *Macromolecular Rapid Communications*, 42(10), Article 2100025.
- Mohammadzadeh, A., Javanbakht, S., & Mohammadi, R. (2024). Magnetic alginate coreshell nanoparticles based on Schiff-base imine bonding for pH-responsive doxorubicin delivery system. Colloids and Surfaces A: Physicochemical and Engineering Aspects, Article 134473.
- Park, H., Weller, C., Vergano, P., & Testin, R. (1993). Permeability and mechanical properties of cellulose-based edible films. *Journal of Food Science*, 58(6), 1361–1364.
- Pawariya, V., De, S., & Dutta, J. (2023). Synthesis and characterization of a new developed modified-chitosan Schiff base with improved antibacterial properties for the removal of Bismarck brown R and Eosin Y dyes from wastewater. Carbohydrate Polymer Technologies and Applications, 6, Article 100352.
- Rakhshaei, R., & Namazi, H. (2017). A potential bioactive wound dressing based on carboxymethyl cellulose/ZnO impregnated MCM-41 nanocomposite hydrogel. Materials Science and Engineering: C, 73, 456–464.
- Ren, J., Xuan, H., Dai, W., Zhu, Y., & Ge, L. (2018). Double network self-healing film based on metal chelation and Schiff-base interaction and its biological activities. *Applied Surface Science*, 448, 609–617.
- Schuren, J., Becker, A., & Gary Sibbald, R. (2005). A liquid film-forming acrylate for periwound protection: A systematic review and meta-analysis (3M™ Cavilon™ no-sting barrier film). *International wound journal*, 2(3), 230–238.
- Shu, Q., Gu, Y., Xia, W., Lu, X., Pang, Y., Teng, J., Liu, B., & Li, Y. (2024). Injectable hydrogels for bioelectronics: A viable alternative to traditional hydrogels. *Chemical Engineering Journal*, Article 153391.
- Sohrabi, H., Javanbakht, S., Oroojalian, F., Rouhani, F., Shaabani, A., Majidi, M. R., Hashemzaei, M., Hanifehpour, Y., Mokhtarzadeh, A., & Morsali, A. (2021). Nanoscale metal-organic frameworks: Recent developments in synthesis, modifications and bioimaging applications. *Chemosphere*, 281, Article 130717.
- Stephen-Haynes, J. (2014). The outcomes of barrier protection in periwound skin and stoma care. *British Journal of Nursing*, 23(Sup5), S26–S30.
- Tawre, M., Padhye, A., Chakraborty, S., Kulkarni, N., Bose, G., Mittal, S., Jadhav, U., Jadhav, S., Rajwade, J., & Pardesi, K. (2024). Bioactive curcuma aromatica-stabilized silver nanoparticles embedded chitosan dressing with improved antibacterial, anti-inflammatory, and wound healing properties. Carbohydrate Polymer Technologies and Applications. Article 100570.
- Tayler, I. M., & Stowers, R. S. (2021). Engineering hydrogels for personalized disease modeling and regenerative medicine. Acta Biomaterialia, 132, 4–22.
- Teng, L., Chen, Y., Jia, Y.-G., & Ren, L. (2019). Supramolecular and dynamic covalent hydrogel scaffolds: From gelation chemistry to enhanced cell retention and cartilage regeneration. *Journal of Materials Chemistry B*, 7(43), 6705–6736.

- Urzedo, A. L., Goncalves, M. C., Nascimento, M. H., Lombello, C. B., Nakazato, G., & Seabra, A. B. (2020). Cytotoxicity and antibacterial activity of alginate hydrogel containing nitric oxide donor and silver nanoparticles for topical applications. ACS Biomaterials Science & Engineering, 6(4), 2117–2134.
- Virzì, N. F., Diaz-Rodriguez, P., Concheiro, A., Pittalà, V., & Alvarez-Lorenzo, C. (2024). Xanthan gum/Guar gum-based 3D-printed scaffolds for wound healing: Production, characterization, and biocompatibility screening. Carbohydrate Polymer Technologies and Applications, Article 100523.
- Wang, H., Hansen, M. B., Löwik, D. W., van Hest, J. C., Li, Y., Jansen, J. A., & Leeuwenburgh, S. C. (2011). Oppositely charged gelatin nanospheres as building blocks for injectable and biodegradable gels. *Advanced materials*, 23(12), H119–H124.
- Wu, Y., Yang, Z., Li, X., Li, T., Zheng, J., Hu, M., Yu, Z., Luo, W., Zhang, W., & Zheng, F. (2023). A self-assembled hydrogel dressing as multi-target therapeutics to promote wound healing. *Chemical Engineering Journal*, 477, Article 147145.
- Wyszogrodzka, G., Marszałek, B., Gil, B., & Dorożyński, P. (2016). Metal-organic frameworks: Mechanisms of antibacterial action and potential applications. *Drug Discovery Today*, 21(6), 1009–1018.
- Yadollahi, M., Namazi, H., & Barkhordari, S. (2014). Preparation and properties of carboxymethyl cellulose/layered double hydroxide bionanocomposite films. *Carbohydrate Polymers*, 108, 83–90.
- Yang, D. (2022). Recent advances in hydrogels (pp. 1987–1989). ACS Publications.
 Zeng, Y., Zhang, C., Du, D., Li, Y., Sun, L., Han, Y., He, X., Dai, J., & Shi, L. (2022). Metalorganic framework-based hydrogel with structurally dynamic properties as a stimuliresponsive localized drug delivery system for cancer therapy. Acta Biomaterialia, 145,
- Zengin, A., Castro, J., Habibovic, P., & Van Rijt, S. (2021). Injectable, self-healing mesoporous silica nanocomposite hydrogels with improved mechanical properties. *Nanoscale*, 13(2), 1144–1154.
- Zhang, X., Liang, Y., Huang, S., & Guo, B. (2024). Chitosan-based self-healing hydrogel dressing for wound healing. Advances in Colloid and Interface Science, Article 103267.
- Zhang, Z., Wang, X., Wang, Y., & Hao, J. (2018). Rapid-forming and self-healing agarose-based hydrogels for tissue adhesives and potential wound dressings. Biomacromolecules, 19(3), 980–988.
- Zhao, H., Liu, M., Zhang, Y., Yin, J., & Pei, R. (2020). Nanocomposite hydrogels for tissue engineering applications. *Nanoscale*, 12(28), 14976–14995.
- Zheng, H., Yang, J., & Han, S. (2016). The synthesis and characteristics of sodium alginate/graphene oxide composite films crosslinked with multivalent cations. *Journal of Applied Polymer Science*, 133(27).
- Zheng, N., Xu, Y., Zhao, Q., & Xie, T. (2021). Dynamic covalent polymer networks: A molecular platform for designing functions beyond chemical recycling and selfhealing. *Chemical Reviews*, 121(3), 1716–1745.
- Zheng, X., Ding, Z., Cheng, W., Lu, Q., Kong, X., Zhou, X., Lu, G., & Kaplan, D. L. (2020).
 Microskin-inspired injectable MSC-laden hydrogels for scarless wound healing with hair follicles. Advanced healthcare materials, 9(10), Article 2000041.